

University of Rhode Island

DigitalCommons@URI

Mechanical, Industrial & Systems Engineering
Faculty Publications

Mechanical, Industrial & Systems Engineering

2017

Persistent Model Order Reduction for Complex Dynamical Systems Using Smooth Orthogonal Decomposition

Shahab Ilbeigi

University of Rhode Island

David Chelidze

University of Rhode Island, chelidze@uri.edu

Follow this and additional works at: https://digitalcommons.uri.edu/mcise_facpubs

Citation/Publisher Attribution

Ilbeigi, S., & Chelidze, D. (2017). Persistent model order reduction for complex dynamical systems using smooth orthogonal decomposition. *Mechanical Systems and Signal Processing*, 96, 125-138. doi:

10.1016/j.ymssp.2017.04.005

Available at: <https://doi.org/10.1016/j.ymssp.2017.04.005>

This Article is brought to you by the University of Rhode Island. It has been accepted for inclusion in Mechanical, Industrial & Systems Engineering Faculty Publications by an authorized administrator of DigitalCommons@URI. For more information, please contact digitalcommons-group@uri.edu. For permission to reuse copyrighted content, contact the author directly.

Persistent Model Order Reduction for Complex Dynamical Systems Using Smooth Orthogonal Decomposition

The University of Rhode Island Faculty have made this article openly available.
Please let us know how Open Access to this research benefits you.

This is a pre-publication author manuscript of the final, published article.

Terms of Use

This article is made available under the terms and conditions applicable towards Open Access Policy Articles, as set forth in our [Terms of Use](#).

Persistent Model Order Reduction for Complex Dynamical Systems Using Smooth Orthogonal Decomposition

Shahab Ilbeigi David Chelidze *

*Department of Mechanical, Industrial, and Systems Engineering
University of Rhode Island, Kingston, RI 02881*

Revised on March 8, 2017

Abstract

Full-scale complex dynamic models are not effective for parametric studies due to the inherent constraints on available computational power and storage resources. A persistent reduced order model (ROM) that is robust, stable, and provides high-fidelity simulations for a relatively wide range of parameters and operating conditions can provide a solution to this problem. The fidelity of a new framework for persistent model order reduction of large and complex dynamical systems is investigated. The framework is validated using several numerical examples including a large linear system and two complex nonlinear systems with material and geometrical nonlinearities. While the framework is used for identifying the robust subspaces obtained from both proper and smooth orthogonal decompositions (POD and SOD, respectively), the results show that SOD outperforms POD in terms of stability, accuracy, and robustness.

Keywords: *nonlinear model reduction, proper orthogonal decomposition, smooth orthogonal decomposition, complex dynamical system, subspace robustness.*

1 Introduction

Considerable progress in computing technology in the past few decades did not alleviate difficulty inherent in simulating complex dynamical systems. Examples of such systems are large-scale finite difference/element, multi-body dynamics, or geometrically nonlinear models, and molecular dynamics simulations [1–6]. A *reduced order model* (ROM) for these systems can be used to significantly reduce redundant computations and data storage requirements [7]. In particular, *persistent* ROMs, which are robust to the changes in system parameters and loading conditions, can be used in parametric studies that are prohibitive when using a full-scale model. While a variety of methods for *model order reduction* (MOR) have been developed, very few of them provide persistent ROMs. Often emphasis is only on the accuracy of the ROMs and their ability to capture the dynamics of the full-scale models for a fixed set of parameters, and operating and loading conditions. However, the importance of the robustness of a ROM to the changes in those parameters is often not accentuated. We consider a ROM to be persistent if it is robust to changes in a full-scale model’s energy,

*email: chelidze@uri.edu ◊ phone: 401.874.2356 ◊ fax: 401.874.2355 ◊ web: mcise.uri.edu/chelidze/

27 forcing, and parameters. Data-based reduced order modeling with no persistency is of limited scope;
28 ROMs built on the data generated from the simulations of a full-scale model can only be used for
29 simulating the same exact configuration of the model. This ROM might still be of great utility if
30 we can study the long-time dynamics of a system (e.g., protein folding), but cannot be utilized in
31 parametric studies, wherein we repeatedly change the parameters, input values, and energy levels.

32 In this paper, we present a new framework for obtaining persistent ROMs, which are valid within
33 a defined range of the system’s energy, which is imposed by changing the input parameters. Our
34 framework can be applied to all data-based MOR methods. We make use of data from simulations
35 or experiments to develop the ROMs. Our goal is to ensure that the obtained persistent ROMs are
36 robust and can be used for simulating the system with any chosen parameter from the defined range.

37

38 1.1 Background and Prior Work

39 Persistent MOR for linear systems has not attracted extensive research focus since the linear modal
40 structure is not dependent on the energy of a system. As a result, if a ROM is properly developed
41 for one energy level of a linear system, it should also be valid for the other energy levels. The
42 methodologies for MOR for these systems are mostly projection based, where the linear subspaces
43 used in the projection can be related to the modal space which is spanned by *linear normal modes*
44 (LNMs). For example, the modes identified using *proper orthogonal decomposition* (POD) (also
45 known as singular value decomposition, principal component analysis, or Karhunen-Loève expansion)
46 [8–12] approximate the LNMs for systems with uniform mass distribution [13]. Other popular
47 methodologies for the MOR of linear systems include the Galerkin reduction using *linear normal*
48 *modes* (LNMs) [14, 15], Krylov subspace projections [16], Hankel norm approximations [17, 18], and
49 truncated balance realizations [19, 20].

50 Nonlinearity, the integral part of complex dynamical systems, makes the development of persis-
51 tent ROMs a much harder problem. Many approaches for nonlinear MOR are based on extending
52 the methodologies used for linear MOR. For example, linearization about an equilibrium point was
53 used for the reduction of weakly nonlinear systems [21, 22]. Many other approaches are derived from
54 POD [8, 9, 11, 23–25], and some from balanced truncation [26–28]. Some other approaches include
55 neural networks [29], Volterra theory [30], and inertial manifold approximation [31]. More recently,
56 a method called Proper Generalized Decomposition (PGD) has been developed as a generalization
57 of POD in order to construct *a priori* ROM [32–35]. This method has a potential for solving multi-
58 dimensional problems since it doesn’t require any knowledge of the solution [34, 36]. The interested
59 reader can find a review on PGD-based MOR techniques in [37].

60 In summary, a majority of the methodologies commonly used for MOR of nonlinear systems
61 can be categorized into two groups. In the first group, *nonlinear normal modes* (NNMs) or their
62 approximations [38–44] are used. In the second group, combined with the Galerkin projection,
63 linear subspaces obtained from spatiotemporal decompositions such as POD and *smooth orthogonal*
64 *decomposition* (SOD) are utilized [2, 9, 10, 25, 45, 46]. Linear subspaces are of considerable current
65 interest because they are computationally tractable and do not neglect the nonlinearity of the original
66 vector-field [8], while, in general, the calculation of NNMs is difficult [47–50]. Also, MOR based on
67 NNMs suffers from another major drawback related to changes in the NNMs with the variation
68 in system’s level of energy [48, 51]. The dependence of the NNMs on the energy level causes an
69 insufficient robustness of the corresponding NNM-based ROMs to the changes in the system’s energy

70 level. Thus, NNM-based ROMs cannot be considered truly persistent.

71 1.2 Our Approach to Persistent Reduced Order Modeling

72 Our approach is based on identifying robust subspaces which do not change drastically as the system
73 changes its energy level. Note that linear subspaces used for MOR are to be identified in such a way
74 that the active NNMs are embedded in them [13]. These subspaces may still change as the NNMs
75 change with the system’s level of energy [51]. However, depending on the decomposition method,
76 some particular subspaces may be robust to variations such as changes in initial conditions, external
77 excitations, energy levels, or systems parameters. Our hypothesis is that while an individual NNM
78 may change with energy, a linear subspace embedding this mode may not undergo any considerable
79 change. Identifying such linear subspaces would enable us to obtain the persistent ROMs that are
80 robust to a relatively wide range of system parameters and operating conditions.

81 The new framework for persistent MOR of large, complex systems based on the concepts of
82 *subspace robustness* and *dynamical consistency* is investigated. These concepts have been recently
83 proposed and discussed in our conference presentations [2, 52, 53], where the MOR subspace ro-
84 bustness for a small dynamical system was evaluated. Subspace robustness characterizes how a
85 linear subspace changes under different conditions of the system, which can be used for complex
86 systems to identify the subspace characteristics that lead to a persistent MOR. Dynamical consi-
87 stency evaluates the deterministic properties of the full-scale system’s trajectory projection onto the
88 corresponding linear subspace. It indicates the ability of the identified subspace to potentially—but
89 not necessarily—result in a stable and accurate ROM.

90 The utility of our framework will be initially evaluated by applying it to the POD subspaces since
91 they are widely used for MOR. POD’s drawback for deterministic systems is that it only considers
92 the statistical (i.e., spatial) characteristics of the data [54]. It only prioritizes the maximal variances
93 in the multivariate data and may disregard important dynamical features that have small variances.
94 Changing the energy level of a system may drastically alter dynamic features that previously had
95 small variances, which will not be reflected in the identified POD modal structure. Therefore, POD,
96 while providing an optimal reduction—in the least squares sense—for a system with fixed set of
97 parameters and forcing, might not be a suitable choice for the persistent MOR of complex systems.
98 The subspace obtained from SOD, which was first used in 2005 for vibration mode identification [54],
99 will also be considered within our framework. SOD can be viewed as an extension of POD, which
100 acquires the ability to separate multivariate data based on inherent characteristic frequencies. In
101 other words, it not only considers the spatial statistics, but also looks at the temporal characteristics
102 of data. Thus, SOD subspaces are likely to be less sensitive to the changes in the energy and
103 properties of the system, and may provide for the persistent MOR.

104 The focus of this study is on complex, nonlinear dynamical systems. However, a lightly damped
105 linear system will be considered first. The rationale behind this consideration is twofold: (1) the
106 assertion that POD recovers LNMs for systems with uniform mass distribution [13] has been only
107 tested on fairly low-dimensional systems, with fairly long time series; and (2) while SOD does not
108 require uniform mass distribution for convergence to the LNMs [54], it has not been tested on
109 large scale systems. Since the LNM structure does not vary with the changes in energy or initial
110 conditions—the corresponding subspaces are robust to these changes—we can use a large-scale linear
111 model to test both the POD and SOD methods’ ability to identify LNMs with limited data in different
112 loading scenarios. In addition, we can also evaluate the ability of these methods to provide robust

113 subspace identification for a system that actually possesses this robustness in all LNMs.

114 Following the example of the linear systems, MOR of two large-scale, complex nonlinear systems
 115 will be studied as the main subject of this paper. POD and SOD will be used for multivariate
 116 analyses of the associated ill-conditioned data matrices from these systems. The POD- and SOD-
 117 spanned subspaces will be tested using the framework to identify the robust subspaces for persistent
 118 ROM development. The resultant ROMs subjected to different energy levels will be simulated using
 119 several numerical examples. The validity of the results will be investigated in terms of the stability
 120 and accuracy of the ROMs.

121 The rest of this paper is organized as follows. In Section 2, the procedure for projection-based
 122 nonlinear model reduction using POD and SOD is reviewed. Section 3 describes the developed
 123 framework for the persistent MOR. In Section 4, the full-scale models of one linear and two nonlinear
 124 systems are described. Results of the ROM simulations are presented and discussed in Section 5,
 125 followed by concluding remarks in Section 6.

126 2 Projection-Based Nonlinear Model Reduction

127 We consider a full-scale model of a deterministic dynamical system that has the following form:

$$\dot{\mathbf{y}} = \mathbf{f}(\mathbf{y}, t), \quad (1)$$

128 where $\mathbf{y} \in \mathbb{R}^{2n}$ is a dynamic state variable, $\mathbf{f} : \mathbb{R}^{2n} \times \mathbb{R} \rightarrow \mathbb{R}^{2n}$ is some nonlinear flow, t is time,
 129 and $n \in \mathbb{N}$ is the number of the system's degrees of freedom. The state variable trajectory data
 130 can be arranged in the matrix $\mathbf{Y} = [\mathbf{y}_1, \mathbf{y}_2, \dots, \mathbf{y}_{2n}]$. A basis for \mathbf{Y} can be estimated using either
 131 the POD or SOD procedures outlined in Ref. [54]. The most dominant k -dimensional basis vectors
 132 are arranged in the matrix $\mathbf{P}_k = [\mathbf{e}_1, \mathbf{e}_2, \dots, \mathbf{e}_k]$. The reduced state variable is obtained using a
 133 coordinate transformation of $\mathbf{q} = \mathbf{P}_k \mathbf{y}$, and the corresponding ROM is:

$$\dot{\mathbf{q}} = \mathbf{P}_k^\dagger \mathbf{f}(\mathbf{P}_k \mathbf{q}, t), \quad (2)$$

134 where $(\cdot)^\dagger$ indicates the pseudoinverse of (\cdot) .

135 2.1 Proper and Smooth Orthogonal Decomposition

136 To build ROMs using the extracted modes from the multivariate analysis, the state variable mea-
 137 surements of the full-scale system are recorded to form position and velocity data matrices $\mathbf{X} \in \mathbb{R}^{r \times n}$
 138 and $\mathbf{V} \in \mathbb{R}^{r \times n}$, respectively. \mathbf{X} is composed of r snapshots of n position state variables. Similarly, \mathbf{V}
 139 is composed of r snapshots of n velocity state variables. Thus, the data matrix \mathbf{Y} , which we call as
 140 full data matrix throughout this paper, is formed by combining \mathbf{X} and \mathbf{V} together, i.e., $\mathbf{Y} = [\mathbf{X} \ \mathbf{V}]$.

141 The time derivative of \mathbf{X} is \mathbf{V} . To obtain a time derivative of \mathbf{V} , or an acceleration data matrix
 142 \mathbf{A} , we can use a full model of our dynamical system, Eq. (1). Alternatively, it can be approximated
 143 by $\mathbf{A} \approx \mathbf{D}\mathbf{V}$, where \mathbf{D} is the matrix form of some differential operator such as forward difference.
 144 Therefore, an ensemble of time derivative of \mathbf{Y} will be $\dot{\mathbf{Y}} = [\mathbf{V} \ \mathbf{A}]$. Provided that \mathbf{Y} and $\dot{\mathbf{Y}}$ are zero
 145 mean, the corresponding auto-covariance matrices can be formed by

$$\Sigma_{yy} = \frac{1}{r-1} \mathbf{Y}^T \mathbf{Y}, \quad \Sigma_{\dot{y}\dot{y}} = \frac{1}{r-1} \dot{\mathbf{Y}}^T \dot{\mathbf{Y}}. \quad (3)$$

146 In POD, we are looking for a basis vector $\phi \in \mathbb{R}^{2n}$ such that a projection of the data matrix
 147 onto this vector has maximal variance. The solution to the POD problem is achieved by solving the
 148 eigenvalue problem of the auto-covariance matrix Σ_{yy} in Eq. (3):

$$\Sigma_{yy}\phi_k = \lambda_k\phi_k, \quad (4)$$

149 where λ_k are proper orthogonal values (POVs), $\phi_k \in \mathbb{R}^{2n}$ are proper orthogonal modes (POMs), and
 150 proper orthogonal coordinates (POCs) are columns of $\mathbf{Q} = \mathbf{Y}\Phi$, in which $\Phi = [\phi_1, \phi_2, \dots, \phi_{2n}] \in$
 151 $\mathbb{R}^{2n \times 2n}$. POVs are ordered such that $\lambda_1 \geq \lambda_2 \geq \dots \geq \lambda_{2n}$, and reflect the variances in \mathbf{Y} data along
 152 the corresponding POMs.

153 In SOD, we are looking for a basis vector $\psi \in \mathbb{R}^{2n}$ such that a projection of the data matrix onto
 154 this vector has both minimal roughness and maximal variance. The solution to the SOD problem,
 155 is achieved by solving a generalized eigenvalue problem of the matrix pair Σ_{yy} and $\Sigma_{\dot{y}\dot{y}}$ in Eq. (3):

$$\Sigma_{yy}\psi_k = \lambda_k\Sigma_{\dot{y}\dot{y}}\psi_k, \quad (5)$$

156 where λ_k are smooth orthogonal values (SOVs), $\psi_k \in \mathbb{R}^{2n}$ are smooth projection modes (SPMs),
 157 smooth orthogonal modes (SOMs) are Ψ^{-T} , and smooth orthogonal coordinates (SOCs) are given
 158 by $\mathbf{Q} = \mathbf{Y}\Psi$, where $\Psi = [\psi_1, \psi_2, \dots, \psi_{2n}] \in \mathbb{R}^{2n \times 2n}$. The degree of smoothness of the coordinates
 159 is described by the magnitude of the corresponding SOV. Thus, the greater in magnitude the SOV,
 160 the smoother in time the corresponding coordinate. It should be noted that if we were to replace
 161 $\Sigma_{\dot{y}\dot{y}}$ with the identity matrix, the formulation would yield the proper orthogonal decomposition.

162 3 Robust Subspace Selection for Persistent MOR

163 The appropriate subspace for model reduction can be selected based on a newly developed criteria [53].
 164 These criteria quantifies two concepts: dynamical consistency—which demonstrates how
 165 well the linear subspace embeds the nonlinear manifold, and subspace robustness—which explains
 166 the sensitivity of the subspace to changes in the system’s level of energy. Here, quantifications of
 167 these concepts are briefly restated. A more complete description can be found in Ref. [53].

168 3.1 Dynamical Consistency

169 The unfolding of an attractor used in delay coordinate embedding [55] is the underlying idea of
 170 dynamical consistency. It can be determined using the premise behind the method of false nearest
 171 neighbors [56]. A linear subspace used for reduced order modeling is said to be dynamically consistent
 172 if the resultant trajectories are deterministic and smooth. The metric for dynamical consistency is
 173 defined as a ratio of the number of false nearest neighbors (FNN) over the total number of nearest
 174 neighbor pairs in a particular k -dimensional subspace:

$$\zeta^k = 1 - \frac{N_{\text{fnn}}^k}{N_{\text{nn}}}, \quad (6)$$

175 where N_{fnn}^k is the estimated number of FNNs in a k -dimensional subspace due to projection, and
 176 N_{nn} is the total number of nearest neighbor pairs used in the estimation. If ζ^k is close to unity, then
 177 that k -dimensional subspace is dynamically consistent.

178 3.2 Subspace Robustness

179 Unlike LNM subspaces that are unique and not sensitive to changes in energy level, the robustness
 180 of the subspaces obtained by multivariate data analysis methods is not guaranteed. In order to

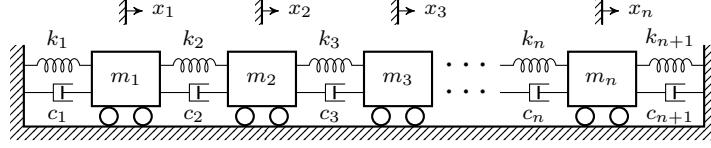


Figure 1: Schematic of the linear system

181 quantify the subspace robustness, the basis vectors which span the k -dimensional subspace for s
 182 system realizations with different levels of energy are concatenated into a matrix $\mathbf{S} \in \mathbb{R}^{2n \times ks}$. Then,
 183 the corresponding subspace robustness γ_s^k is given by the following expression:

$$\gamma_s^k = \left| 1 - \frac{4}{\pi} \arctan \frac{\sum_{i=k+1}^{2n} \sigma_i^2}{\sum_{i=1}^k \sigma_i^2} \right|, \quad (7)$$

184 where σ_i 's are proper orthogonal values of the matrix \mathbf{S} . If all the subspaces embedded in \mathbf{S} are
 185 spanning the same subspace, then $\gamma = 1$.

186 4 Full-scale Models

187 Complexity in dynamical systems can arise for different reasons. In nonlinear dynamical systems,
 188 it can be related to the size, nonlinearity, or a weak coupling between the DOFs resulting in simul-
 189 taneous presence of slow and fast dynamics. Here we study one large linear system as well as two
 190 nonlinear systems.

191 The linear system under investigation is an n -degree-of-freedom mass-spring-damper system, as
 192 shown in Fig. 1, where n blocks of masses are connected in series to each other, as well as both
 193 sides of the support, by linear dampers and springs. The masses can vibrate in x -direction with no
 194 friction. The system is described by the following governing differential equations:

$$\begin{cases} m_i \ddot{x}_i + (c_i + c_{i+1}) \dot{x}_i - c_{i+1} \dot{x}_{i+1} + \\ (k_i + k_{i+1}) x_i - k_{i+1} x_{i+1} = f_i(t), & \text{for } i = 1; \\ \\ m_i \ddot{x}_i - c_i \dot{x}_{i-1} + (c_i + c_{i+1}) \dot{x}_i - c_{i+1} \dot{x}_{i+1} \\ - k_i x_{i-1} + (k_i + k_{i+1}) x_i - k_{i+1} x_{i+1} = f_i(t), & \text{for } 2 \leq i \leq n-1; \\ \\ m_i \ddot{x}_i - c_i \dot{x}_{i-1} + (c_i + c_{i+1}) \dot{x}_i - k_i x_{i-1} + \\ (k_i + k_{i+1}) x_i = f_i(t), & \text{for } i = n, \end{cases} \quad (8)$$

195 where $n \in \mathbb{N}$ is the number of the system's degrees of freedom and $f_i(t)$ is the external forcing
 196 applied to the i -th mass. Defining $\mathbf{z} = [\{x_i\}_{i=1}^n, \{\dot{x}_i\}_{i=1}^n]^T$ as the vector of $2n$ state variables, the
 197 full state-space model of the system can be obtained as follows:

$$\dot{\mathbf{z}} = \begin{bmatrix} \mathbf{0} & \mathbf{I} \\ -\mathbf{M}^{-1}\mathbf{K} & -\mathbf{M}^{-1}\mathbf{C} \end{bmatrix} \mathbf{z} + \mathbf{f}_e(t), \quad (9)$$

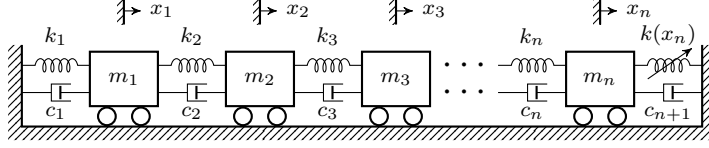


Figure 2: Schematic of the system with nonlinear spring coupling

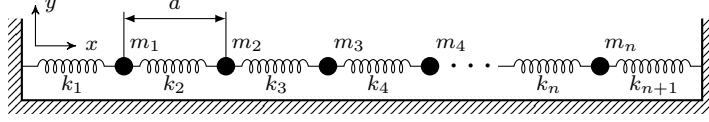


Figure 3: Schematic the mass-spring-grid system with geometric nonlinearity

198 where $\mathbf{f}_e(t) = [[0, \dots, 0]_{1 \times n}, [1, \dots, 1]_{1 \times n}]^T$; $\mathbf{0} \in \mathbb{R}^{n \times n}$ is a zero matrix; $\mathbf{I} \in \mathbb{R}^{n \times n}$ is an identity
 199 matrix; and \mathbf{M} , \mathbf{K} , and \mathbf{C} are $n \times n$ mass, stiffness, and damping matrices, respectively.

200 The first nonlinear system used here is obtained by adding a nonlinear spring to the linear
 201 system as shown in Fig. 2. In this case, the complexity is caused by the large size as well as the
 202 material nonlinearity. The system dynamics are described by the following full state-space equations
 203 of motion:

$$\dot{\mathbf{z}} = \begin{bmatrix} \mathbf{0} & \mathbf{I} \\ -\mathbf{M}^{-1}\mathbf{K} & -\mathbf{M}^{-1}\mathbf{C} \end{bmatrix} \mathbf{z} + \mathbf{f}_e + \mathbf{f}_{\text{nonlinear}}(\mathbf{z}), \quad (10)$$

204 where everything is the same as for the linear model except except nonlinear term $\mathbf{f}_{\text{nonlinear}}(\mathbf{z}) \in \mathbb{R}^{2n}$, which
 205 has only one nonzero element: $[\mathbf{f}_{\text{nonlinear}}(\mathbf{z})]_{2n} = -\alpha z_n^3$.

206 The third system will be called the mass-spring-grid system throughout this paper. It has the
 207 same design and arrangement as the first system, but with a pretension in the springs. Each spring
 208 is assumed to have a corresponding damper acting in parallel. The system is allowed to vibrate in
 209 both x and y directions as a grid of equidistant masses, dampers, and springs shown in Fig. 3. In
 210 case the system is forced only in the x -direction, Eq. (8) is sufficient to describe it. However, any
 211 small deviation from x -directional oscillation will cause geometric nonlinearity in the motion. For
 212 the purpose of this paper, we only excite this system in the y -direction. The governing differential
 213 equations for each i -th mass are given in Appendix A.

214 The state-space vector to model this system is a vector of $4n$ variables defined as $\mathbf{z} = [\{y_i\}_{i=1}^n,$
 215 $\{x_i\}_{i=1}^n, \{\dot{y}_i\}_{i=1}^n, \{\dot{x}_i\}_{i=1}^n]^T \in \mathbb{R}^{4n}$. Thus, Eq. (15) and Eq. (18) from the appendix can be rewritten
 216 as follows:

$$\dot{\mathbf{z}} = \begin{bmatrix} \mathbf{0} & \mathbf{0} & \mathbf{I} & \mathbf{0} \\ \mathbf{0} & \mathbf{0} & \mathbf{0} & \mathbf{I} \\ -\mathbf{M}^{-1}\mathbf{K} & \mathbf{0} & -\mathbf{M}^{-1}\mathbf{C} & \mathbf{0} \\ \mathbf{0} & -\mathbf{M}^{-1}\mathbf{K} & \mathbf{0} & -\mathbf{M}^{-1}\mathbf{C} \end{bmatrix} \mathbf{z} + \begin{bmatrix} \mathbf{0}_{n \times 1} \\ \mathbf{0}_{n \times 1} \\ \mathbf{f}_{n,y} \\ \mathbf{f}_{n,x} \end{bmatrix} + \mathbf{f}_e, \quad (11)$$

217 where $\mathbf{f}_{n,y}$, $\mathbf{f}_{n,x}$, and \mathbf{f}_e are given in Appendix A; and $\mathbf{0}$, \mathbf{I} , \mathbf{M} , \mathbf{K} , and \mathbf{C} are $n \times n$ zero, identity,
 218 mass, stiffness, and damping matrices, respectively.
 219

220 5 Results and Discussion

221 The MOR objective is to develop persistent ROMs for *harmonically excited* systems considered in
 222 this paper. These systems will be excited by a force with frequency close to the first natural frequency

223 of the corresponding linear(ized) system. Modal subspaces for model reduction can be obtained from
 224 different types of excitations, including both harmonic and random. With random forcing, we are
 225 more likely to explore nearly all the state-space of the system and excite all dominant frequencies.
 226 However, the particular forcing function has to be carefully selected, especially for the systems that
 227 have combined slow and fast dynamics. This is to limit the contamination of the identified modes
 228 by forcing that can obscure the true modal structure of the system.

229 For the first and the second system, white noise is used to excite the system because there are
 230 no relatively fast dynamics in the presence of slow dynamics. For the third system, we use colored
 231 white noise with the cut-off frequency of 6 Hz, which, for our numerical example, will be around the
 232 frequency of the linearized system's ninth LNM. This allows the excitation of lower modal frequencies,
 233 while limiting contamination from high frequency modes that do not get excited in practice. Also,
 234 the external excitation containing a range of frequencies ensures that the geometrical nonlinearity
 235 caused by the x -direction oscillations is observable while these oscillations are not contaminated by
 236 noise.

237 We did 12 independent simulations for each system subjected to external stochastic excitations.
 238 The obtained time series from each simulation had different levels of energy imposed by changing the
 239 amplitude of forcing. For fair comparison purposes, we need to be consistent with the selection of the
 240 total simulation time for each system. Thus, each simulation was done for a total time equal to 100
 241 cycles of a harmonic forcing, with the frequency equal to 110% of the first natural frequency of the
 242 corresponding linearized system. With the chosen parameters for the systems, the total simulation
 243 times were equal to 709.8 sec for the linear, 495.1 sec for the nonlinear spring, and 120.8 sec for the
 244 mass-spring-grid systems. We recorded 100 data samples in each cycle of applied external forcing.
 245 Therefore, a total of 10,000 data points were recorded from each simulation.

246 In each case, POD and SOD were used to extract the modes out of each data set. The first k dom-
 247 inant modes identified from each simulation independently, spanning 12 k -dimensional subspaces,
 248 were concatenated into the matrix \mathbf{S} as explained in Section 3.2. Singular value decomposition was
 249 applied to matrix \mathbf{S} in order to extract the singular modes and the corresponding singular values.
 250 Using singular values and Eq. (7), the robustness of the k -dimensional subspaces were evaluated for
 251 each model and decomposition scheme.

252 The corresponding singular modes were used to obtain projections of the full-scale models' har-
 253 monically excited trajectories onto them. Using the procedure outlined in Section 3.1, the dynamical
 254 consistency of the resulting trajectories for all the k -dimensional subspaces in the full n -dimensional
 255 vector space were obtained. Please note that no matter how we obtain the subspace for model
 256 reduction, the calculation of the dynamical consistency is meaningful only for the deterministic
 257 trajectories. The dynamical consistencies were obtained for five deterministic trajectories, each cor-
 258 responding to different forcing amplitudes, and then averaged out. In case both subspace robustness
 259 and dynamical consistencies of the extracted modes were close to unity, we considered them as
 260 suitable for persistent MOR.

261 The parameters of the linear system were fixed as follows:

$$n = 100, m = 1 \text{ kg}, k = 1000 \text{ N/M}, c = 0.048 \text{ N} \cdot \text{M/s}. \quad (12)$$

262 The obtained POMs and SOMs for this system are used to get the subspace robustness and dynamical
 263 consistency of the ROM subspaces. For the randomly driven linear system, as depicted in Fig. 4,
 264 the SOD subspace robustness metric reaches and stays close to unity for $k \geq 3$. POD subspace
 265 robustness is close to unity at $k = 2$ and $k = 3$. It drops at $k = 4$ and again reaches unity at $k = 25$

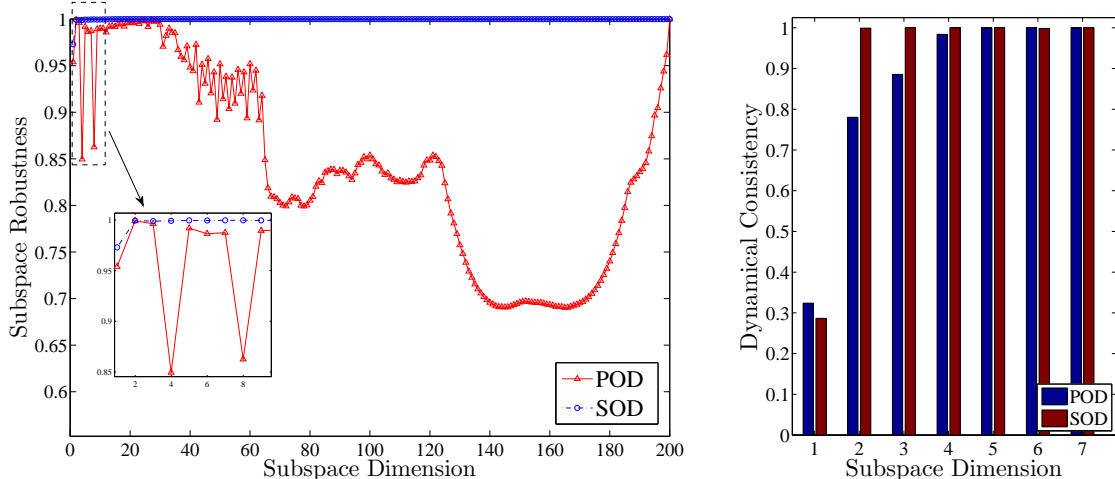


Figure 4: Subspace robustness (left) and dynamical consistency (right) for randomly driven linear system

266 in a non-monotonic manner.

267 The POD subspace robustness does not behave monotonically and does not stay close to unity
 268 once it reaches it. Therefore, in the cases considered, POMs cannot approximate fixed LNMs in a
 269 robust manner, except maybe a few lower modes. This shows that POMs are not robust under the
 270 limited time-history constraints of high-dimensional data, which makes them unreliable for persistent
 271 MOR. In contrast, the SOD subspace robustness monotonically increases, reaches unity for a low
 272 dimension, and does not fluctuate thereafter.

273 Figure 4 also shows the dynamical consistency of POD- and SOD-based subspaces for the ran-
 274 domly driven linear system. For both POD and SOD, the dynamical consistencies are similar
 275 reaching unity at $k = 2$ for SOD and $k = 5$ for POD. This means that the projection of the linear
 276 system’s deterministic trajectories onto the five-dimensional POD-based, or the two-dimensional
 277 SOD-based, dominant subspaces has no singular point or intersection with itself—or, they do not
 278 violate the uniqueness of the deterministic evolution.

279 The linear system subjected to harmonic excitation was simulated using the POD- and SOD-
 280 based ROMs via Eq. (2). The phase portraits for the vibrations of the thirtieth mass are depicted
 281 in Fig. 5 and Fig. 6. The ROM simulations results show a very good visual correspondence to
 282 the full-scale system using both POD and SOD. Both methods are able to capture the dynamics
 283 in two- and three-dimensional ROMs and none of them outperformed the other irrespective of the
 284 robustness of the corresponding subspaces.

285 A question arises as to why some relatively non-robust POD subspace-based ROMs, like the four-
 286 dimensional model, still correlate with the full-scale model. It should be noted that the subspace
 287 robustness metric is of more importance for lower dimensions, since they possess most of the energy
 288 of the system. The two- and three-dimensional POD subspaces for the linear system are robust
 289 and capture most of the system’s energy, thus providing for good ROMs of the system. Increasing
 290 the dimension of the ROM reduces the robustness of the associated POD subspace to 0.85 but it
 291 does not affect its accuracy or stability. This is mainly due to the fact that the fourth POM does
 292 not capture enough associated energy to have a sizable effect on the corresponding ROM. This also
 293 explains why the robustness of MOR based on POD has not been of much research concern for linear
 294 systems. As shown in Fig. 7, POD captures most of the energy in the very first few modes, which
 295 are robust to the changes in the energy of the system. Therefore, any suitably developed POD-based

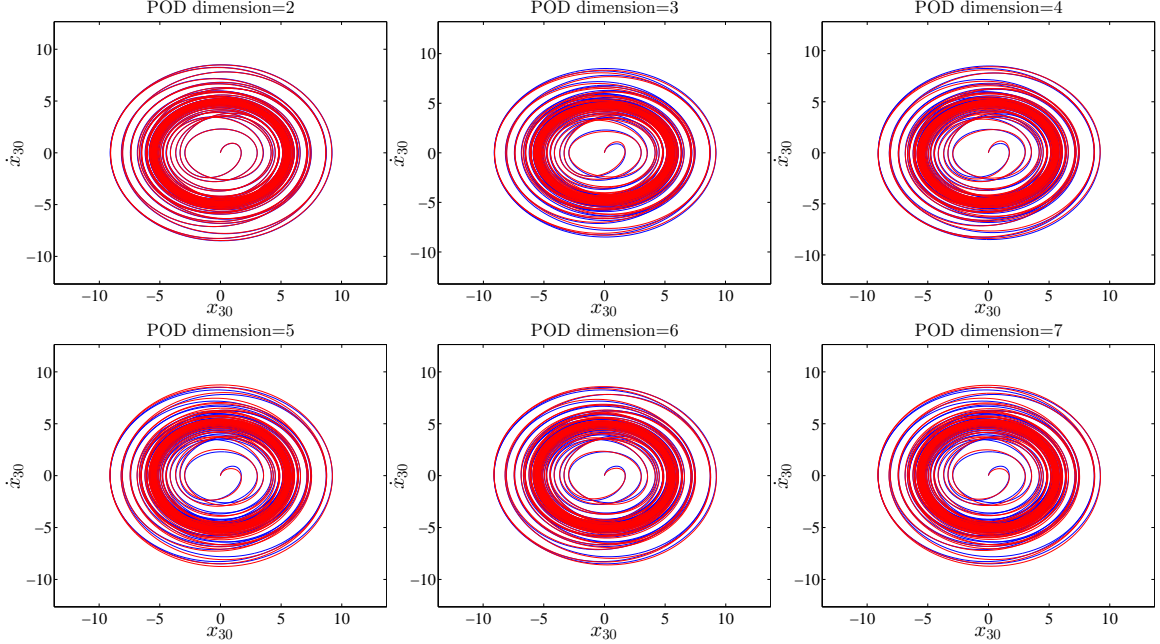


Figure 5: POD-based ROMs of the linear system for $\Omega = 5.52$ Hz and $q_0 = 1$

296 ROM could probably account for other similar conditions.

297 ROMs for nonlinear systems are expected to be more sensitive to the robustness of the cor-
 298 responding MOR linear subspaces. Therefore, in case the low-dimensional subspaces have good
 299 robustness, the non-robust higher dimensional subspace may destabilize the numerical scheme for
 300 the model, or at least adversely affect its accuracy.

301 For investigation of the system with nonlinear spring coupling, the number of DOFs was set to
 302 60 and the other parameters were fixed as follows:

$$m = 1 \text{ kg}, k = 3600 \text{ N/M}, c = 720 \text{ N.M/s}, \alpha = 2. \quad (13)$$

303 This results in a rich dynamic response with two stable and one unstable static equilibrium points.
 304 Subjected to harmonic forcing with $\Omega = 9.97$ Hz, and using the forcing amplitude as a bifurcation
 305 parameter, the corresponding bifurcation diagram is plotted using the full scale model of the system
 306 as shown in Fig. 8. Our particular aim for the persistent ROM is to reproduce these bifurcation
 307 results, which will demonstrate robustness of ROM over a range of forcing amplitudes or different
 308 input energy levels.

309 The subspace robustness and dynamical consistency for this system are depicted in Fig. 9. The
 310 robustness for the SOD subspaces reaches unity at $k = 4$, while for POD it does not happen until
 311 the very end. POD subspace robustness is fluctuating and sometimes getting worse as the subspace
 312 dimension increases. These fluctuations are of greater importance for lower dimensional subspaces
 313 since most of the system's response energy is captured in these subspaces. The dynamical consistency
 314 for both methods is similar and reaches unity at $k = 2$. At $k = 5$, however, the dynamical consistency
 315 of the SOD method slightly drops, which may affect the accuracy of the corresponding ROM.

316 While two- and three-dimensional POD subspace robustness are relatively close to unity, they
 317 do not account for a significant portion of the system's total energy to provide stable ROMs. The
 318 robustness of the four-dimensional POD subspace is low, which causes the diverging results of the

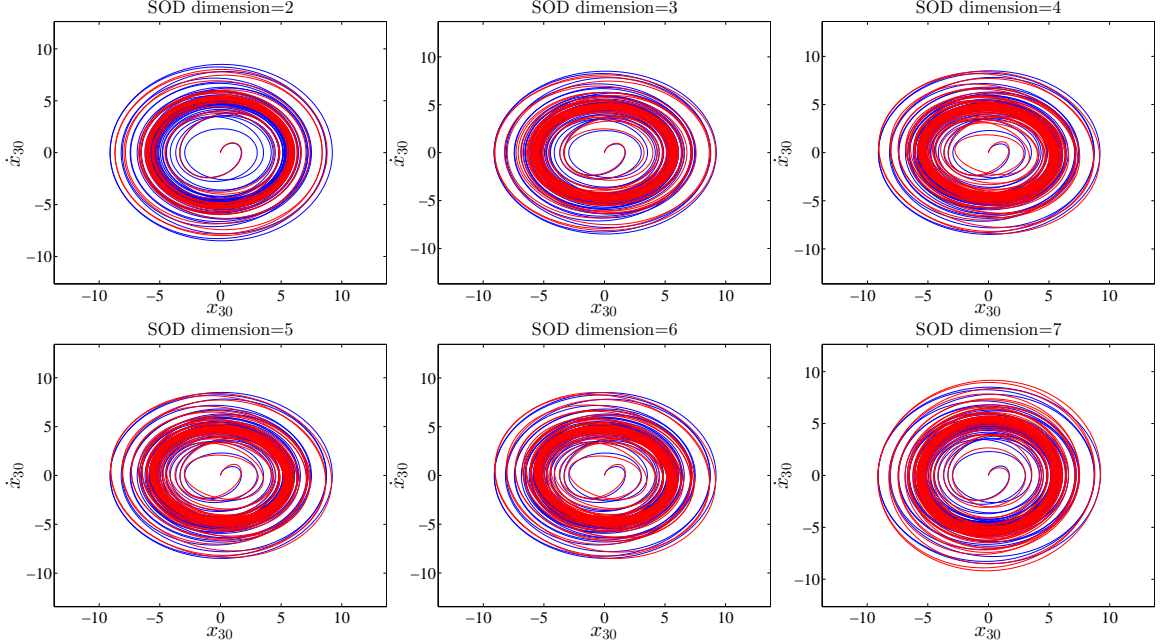


Figure 6: SOD-based ROMs of the linear system for $\Omega = 5.52$ Hz and $q_0 = 1$

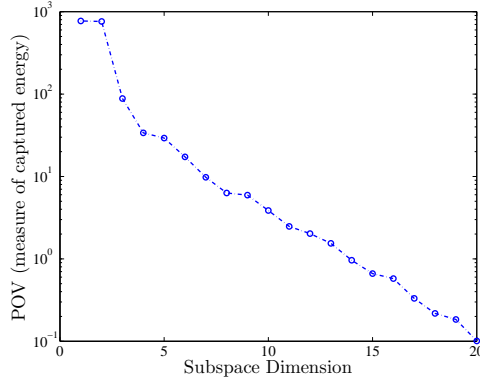


Figure 7: Captured energy versus number of the modes for the linear system

319 corresponding ROM simulation. The five-dimensional POD subspace has better robustness, and the
 320 simulations showed that it provides stable ROM, yet is not robust enough to accurately reproduce
 321 the bifurcation diagram. Since the six-dimensional POD-based ROM has better robustness and
 322 captures more energy, it results in stable and accurate simulations.

323 One- through three-dimensional SOD subspaces do not result in persistent ROMs because their
 324 subspace robustness is relatively low and also they do not capture enough energy of the system.
 325 Four- and higher-dimensional SOD subspaces are robust and provide persistent ROMs capable of
 326 reproducing the bifurcation diagram of the full-scale system.

327 The lowest dimensional ROM which provides accurate and robust results is four-dimensional for
 328 SOD and six-dimensional for POD. The corresponding bifurcation diagrams are shown in Fig. 10.
 329 These ROMs are more than fifty times faster in simulation than the full scale model. Thus, we used
 330 a finer increment size for the forcing amplitude to provide more details in the bifurcation diagrams
 331 of the system. Comparing these diagrams with the reference diagram shown in Fig. 8, there is a

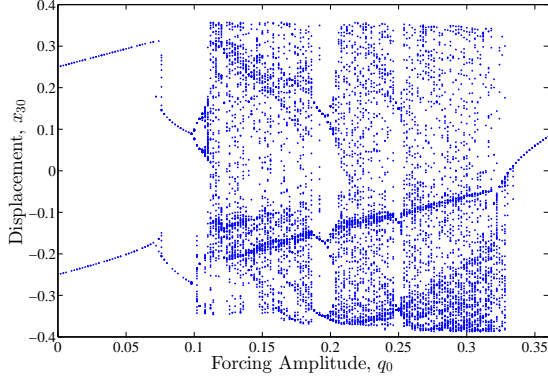


Figure 8: Bifurcation diagram for full scale nonlinear system for harmonic forcing with $\omega = 9.97$ Hz

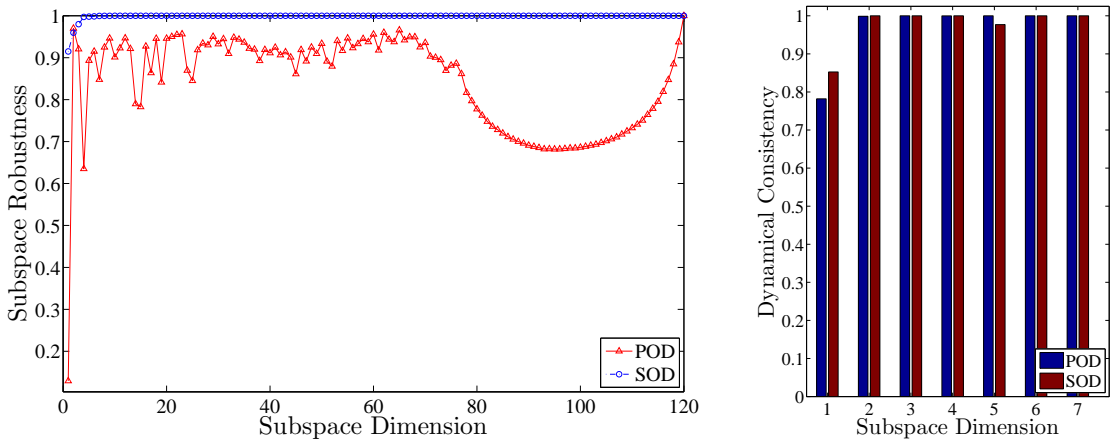


Figure 9: Subspace robustness (left) and dynamical consistency (right) for randomly driven nonlinear system

332 close match between those of the six-dimensional POD and the full scale model. For the SOD,
 333 the bifurcation diagram is little shrunk around $q_0 = 0.33$. While this bifurcation diagram is not
 334 strictly accurate, it still provides a faithful qualitative description the full-scale system’s dynamics.
 335 In addition, the results for the six-dimensional SOD are as good as the six-dimensional POD, while
 336 the test shows that the four-dimensional POD is not even stable, due to the significant drop of its
 337 subspace robustness at $k = 4$.

338 In Fig. 11, six-dimensional POD and four-dimensional SOD ROMs are compared to the full-scale
 339 model driven by the harmonic forcing with $\Omega = 9.97$ Hz and amplitudes of 0.05, 0.14, 0.28, and 0.35.
 340 The four-dimensional SOD model successfully competes with the six-dimensional POD model. For
 341 smaller amplitudes, four-dimensional SOD even outperforms the six-dimensional POD. In addition,
 342 Fig. 12 shows how the relative accuracy of the SOD-based ROMs drops for $k = 5$ as compared to
 343 $k = 4$ and 6. This can be explained by the drop in the dynamical consistency of SOD for $k = 5$,
 344 which was shown in Fig. 9.

345 For the mass-spring-grid system consisting of twenty masses, specifying the following parameters
 346 will result in a rich dynamical behavior:

$$n = 20, m = 1 \text{ kg}, k = 1000 \text{ N/M}, c = 4.23 \text{ N.M/s}, a = 1.01 \text{ m}, l = 1 \text{ m}. \quad (14)$$

347 The subspace robustness for POD-based MOR of this system is close to unity for $k = 1, \dots, 4$ and

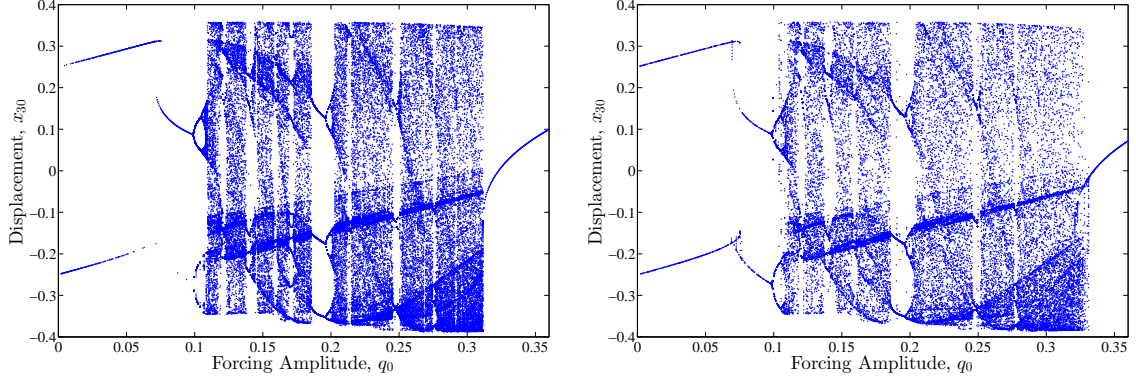


Figure 10: Bifurcation diagram for ROMs of the nonlinear system for harmonic forcing with $\omega = 9.97$ Hz : four-dimensional SOD (left); six-dimensional POD (right)

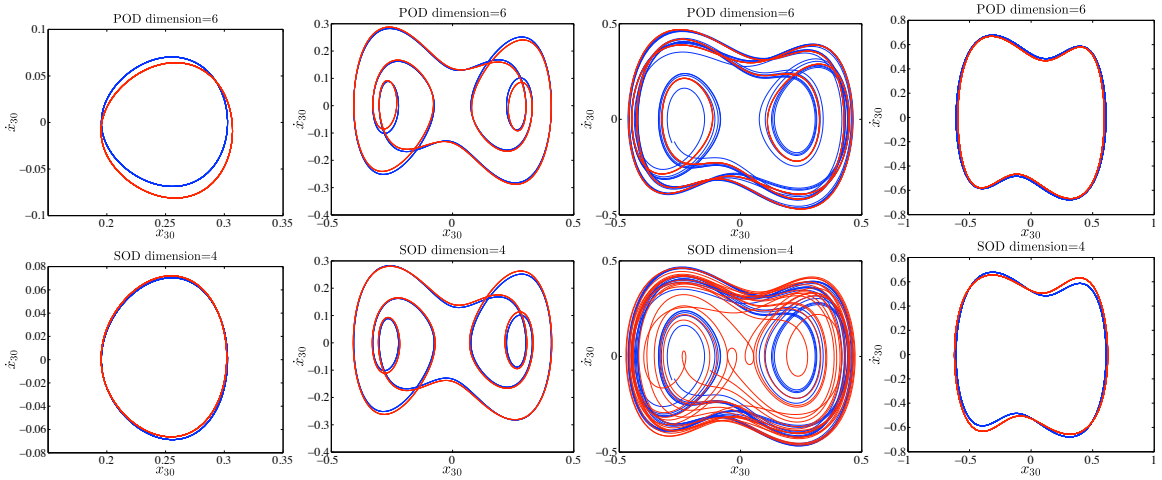


Figure 11: Phase portraits of the 30-th mass of the nonlinear system obtained from full scale (blue) and reduced order models (red): four-dimensional POD-based ROMs (top); six-dimensional SOD-based ROMs (bottom)

348 drops to 0.6 at $k = 5$, as shown in Fig. 13. For SOD, subspace robustness starts at near 0.85 for
 349 $k = 1$, monotonically increases with the increase in the dimension, and saturates at 1 near $k = 20$.
 350 Also, three- and higher-dimensional POD-based ROMs are dynamically consistent, while for SOD,
 351 five- and higher-dimensional subspaces are dynamically consistent. The importance of subspace
 352 robustness and dynamical consistency metrics for identifying the optimal MOR subspace is reflected
 353 in Fig. 14, where POD-based ROMs lose their stability as subspace robustness drops for $k = 5$.
 354 While the five-dimensional ROM is still stable, for the $k = 6, 7$, or 8 , it loses its stability. The
 355 importance of monotonically increasing subspace robustness for SOD-based ROMs is illustrated in
 356 Fig. 15. These ROMs become and remain stable as the robustness metric approaches unity and
 357 stays there.

358 Therefore, for all the three types of systems under investigation, the subspace robustness and
 359 dynamical consistency of the ROMs were good indicators for the stability, accuracy, and reliability
 360 of the corresponding ROMs. Not only does any deviation of these metrics from unity reduce the
 361 accuracy, but it may also destabilize the corresponding ROMs. In particular, in contrast to POD,
 362 when SOD-based ROMs become stable, they stay stable for higher dimensional reductions. This
 363 is directly correlated with monotonic improvement in the SOD subspace robustness, which also

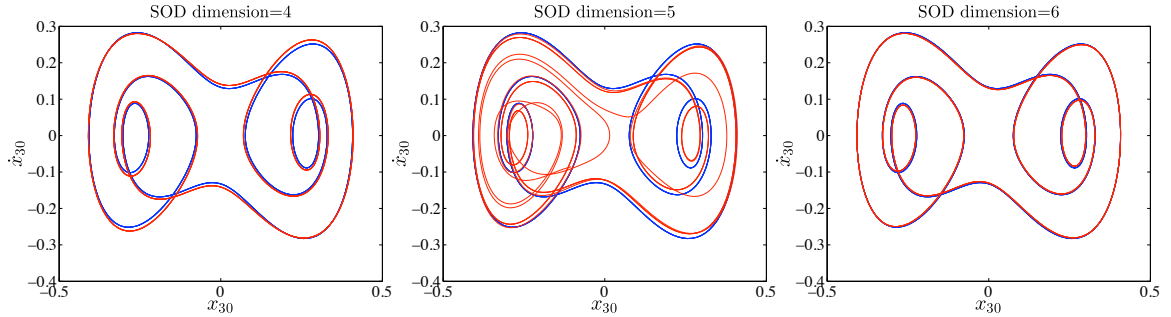


Figure 12: Phase portraits of the 30-th mass of the nonlinear system obtained from full scale (blue) and SOD-based ROMS (red)

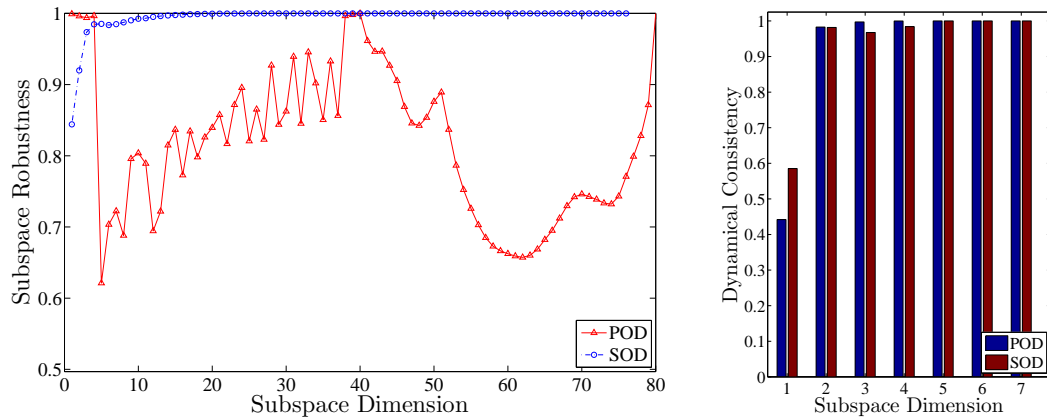


Figure 13: Subspace robustness (left) and averaged dynamical consistency (right) for randomly driven nonlinear mass-grid system

364 correlates with the improved accuracy of the corresponding ROMs. For the POD subspaces, we do
 365 not observe this monotonic increase in the robustness, which may drop precipitously as the subspace
 366 dimension increases. This may cause the loss of stability in the corresponding ROM for the nonlinear
 367 dynamical system.

368 The performance of the studied framework for identifying the optimal subspaces for persistent
 369 MOR was verified by reproducing full scale model simulations for a range of amplitudes and frequen-
 370 cies of external excitation, and initial conditions. For the second and the third system, where more
 371 complexities were introduced through material and geometrical nonlinearities, the SOD-based model
 372 outperformed the POD-based models by providing more consistent and persistent reductions. Also,
 373 we should emphasize that the obtained fast, stable, and robust-over-a-wide-energy-range ROMs
 374 enabled us to study these systems in more detail.

375 6 Conclusions

376 A persistent MOR for dynamical systems was investigated for one example of a large linear system
 377 and two examples of large and complex nonlinear systems. A framework based on subspace robust-
 378 ness and dynamical consistency was shown to be successful in identifying the robust subspaces for
 379 the development of persistent ROMs. To verify the performance of the framework, the simulation
 380 results of the full scale models were reproduced using the ROMs. In particular, SOD-based ROMs

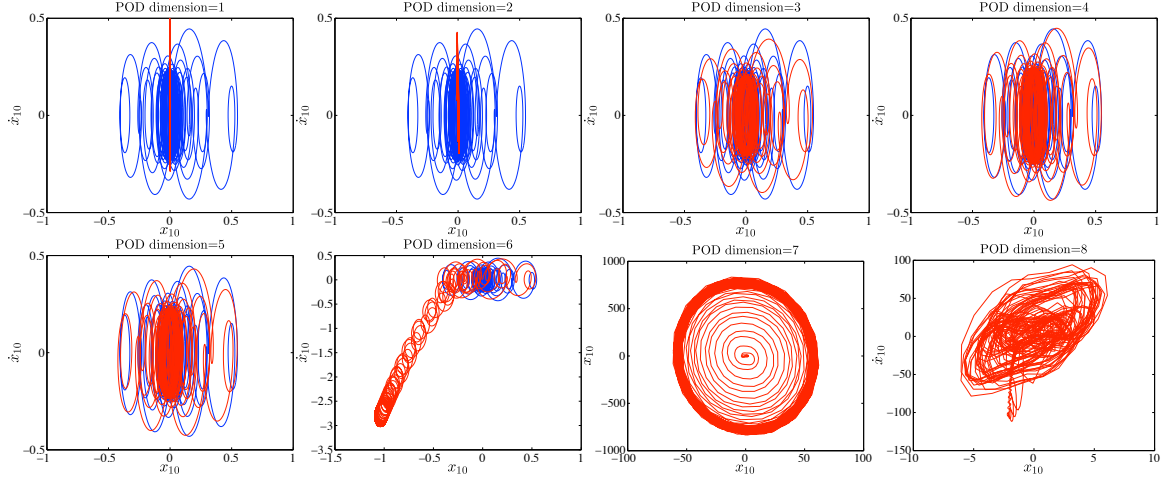


Figure 14: Phase portraits of the 10-th mass of the nonlinear mass-grid system obtained from full scale model (blue) for $\Omega = 28.2\text{ Hz}$ and $q_0 = 1$ compared to 1- through 8-dimensional POD-based ROMs (red)

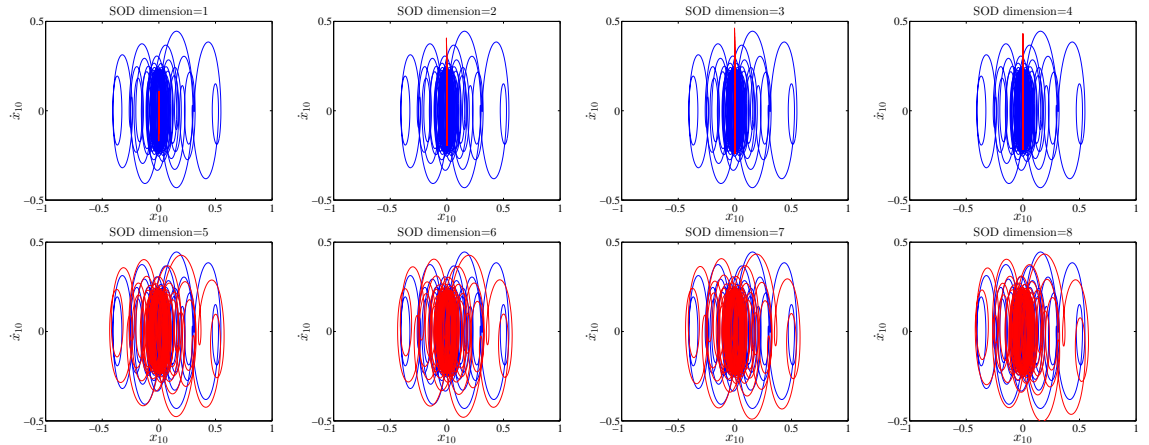


Figure 15: Phase portraits of the 10-th mass of the nonlinear mass-grid system obtained from full scale model (blue) for $\Omega = 28.2\text{ Hz}$ and $q_0 = 1$ compared to 1- through 8-dimensional SOD-based ROMs (red)

381 outperformed the POD-based ones in terms of the stability and robustness of the model. Also,
 382 the obtained persistent ROMs could be successfully used to study the dynamics of computationally
 383 expensive complex models for a relatively wide range of parameters and conditions.

384 The persistent MOR framework presented in this paper can be used for improving all the
 385 projection-based methods and has a good performance for parametric studies within their domain of
 386 interest. However, the parametric study is only limited to the defined range of parameters and the
 387 persistent model is expected to be valid only in this range. In our study, we focused on a *relatively*
 388 *wide* range of parameters where the complex systems exhibit interesting dynamics, which includes
 389 linearity, nonlinearity, periodicity, intermittence, and chaos. In future work, one needs to study the
 390 validity of persistent ROMs outside the domain of interest. Future efforts may focus on increasing
 391 the size of the domain for persistent MOR.

Acknowledgement

This paper is based upon work supported by the National Science Foundation under Grant No. 1100031.

References

- [1] Benner, P., Mehrmann, V., and Sorensen, D. C., 2005. *Dimension reduction of large-scale systems*, vol. 45. Springer.
- [2] Ilbeigi, S., and Chelidze, D., 2016. “Model order reduction of nonlinear euler-bernoulli beam”. In *Nonlinear Dynamics, Volume 1*. Springer, pp. 377–385.
- [3] Antoulas, A. C., Ionutiu, R., Martins, N., ter Maten, E. J. W., Mohaghegh, K., Pulch, R., Rommes, J., Saadvandi, M., and Striebel, M., 2015. “Model order reduction methods, concepts and properties”.
- [4] Maier, D., Hager, C., Hetzler, H., Fillot, N., Vergne, P., Dureisseix, D., and Seemann, W., 2015. “A nonlinear model order reduction approach to the elasto-hydrodynamic problem”. *Tribology International*, **82**, pp. 484–492.
- [5] Kudryavtsev, M., Rudnyi, E., Korvink, J., Hohlfeld, D., and Bechtold, T., 2015. “Computationally efficient and stable order reduction methods for a large-scale model of mems piezoelectric energy harvester”. *Microelectronics Reliability*, **55** (5), pp. 747–757.
- [6] Benner, P., and Feng, L. “Model order reduction for coupled problems”.
- [7] Balajewicz, M., Amsallem, D., and Farhat, C., 2015. “Projection-based model reduction for contact problems”. *arXiv preprint arXiv:1503.01000*.
- [8] Rathinam, M., and Petzold, L. R., 2003. “A new look at proper orthogonal decomposition”. *SIAM Journal on Numerical Analysis*, **41** (5), pp. 1893–1925.
- [9] Willcox, K., and Peraire, J., 2002. “Balanced model reduction via the proper orthogonal decomposition”. *AIAA journal*, **40** (11), pp. 2323–2330.
- [10] Benner, P., and Breiten, T., 2015. “Two-sided projection methods for nonlinear model order reduction”. *SIAM Journal on Scientific Computing*, **37** (2), pp. B239–B260.
- [11] Georgiou, I., 2005. “Advanced proper orthogonal decomposition tools: using reduced order models to identify normal modes of vibration and slow invariant manifolds in the dynamics of planar nonlinear rods”. *Nonlinear dynamics*, **41** (1-3), pp. 69–110.
- [12] Ghasemi, M., Yang, Y., Gildin, E., Efendiev, Y., Calo, V., et al., 2015. “Fast multiscale reservoir simulations using pod-deim model reduction”. In *SPE Reservoir Simulation Symposium*, Society of Petroleum Engineers.
- [13] Kerschen, G., Golinval, J.-c., Vakakis, A. F., and Bergman, L. A., 2005. “The method of proper orthogonal decomposition for dynamical characterization and order reduction of mechanical systems: an overview”. *Nonlinear dynamics*, **41** (1-3), pp. 147–169.
- [14] Foias, C., Jolly, M., Kevrekidis, I., Sell, G., and Titi, E., 1988. “On the computation of inertial manifolds”. *Physics Letters A*, **131** (7), pp. 433–436.

- 428 [15] Pesheck, E., Pierre, C., and Shaw, S., 2002. “A new galerkin-based approach for accurate non-
429 linear normal modes through invariant manifolds”. *Journal of sound and vibration*, **249** (5),
430 pp. 971–993.
- 431 [16] Feldmann, P., and Freund, R. W., 1995. “Efficient linear circuit analysis by padé approximation
432 via the lanczos process”. *Computer-Aided Design of Integrated Circuits and Systems*, *IEEE*
433 *Transactions on*, **14** (5), pp. 639–649.
- 434 [17] Glover, K., 1984. “All optimal hankel-norm approximations of linear multivariable systems and
435 their l₁-error bounds”. *International journal of control*, **39** (6), pp. 1115–1193.
- 436 [18] Zhou, H., Su, X., Song, Y.-D., and Yan, Q., 2015. “Hankel-norm model reduction for de-
437 layed fuzzy systems”. In *Control and Decision Conference (CCDC)*, 2015 27th Chinese, *IEEE*,
438 pp. 964–968.
- 439 [19] Phillips, J. R., Daniel, L., and Silveira, L. M., 2003. “Guaranteed passive balancing transforma-
440 tions for model order reduction”. *Computer-Aided Design of Integrated Circuits and Systems*,
441 *IEEE Transactions on*, **22** (8), pp. 1027–1041.
- 442 [20] Baur, U., Benner, P., and Feng, L., 2014. “Model order reduction for linear and nonlinear
443 systems: a system-theoretic perspective”. *Archives of Computational Methods in Engineering*,
444 **21** (4), pp. 331–358.
- 445 [21] Bai, Z., 2002. “Krylov subspace techniques for reduced-order modeling of large-scale dynamical
446 systems”. *Applied numerical mathematics*, **43** (1-2), pp. 9–44.
- 447 [22] Phillips, J. R., 2003. “Projection-based approaches for model reduction of weakly nonlinear,
448 time-varying systems”. *IEEE Transactions on computer-aided design of integrated circuits and*
449 *systems*, **22** (2), pp. 171–187.
- 450 [23] Broomhead, D., and Kirby, M., 2005. “Dimensionality reduction using secant-based projection
451 methods: The induced dynamics in projected systems”. *Nonlinear Dynamics*, **41** (1) , pp. 47–67.
- 452 [24] Glösmann, P., and Kreuzer, E., 2005. “Nonlinear system analysis with karhunen–loève trans-
453 form”. *Nonlinear Dynamics*, **41** (1) , pp. 111–128.
- 454 [25] Smith, T. R., Moehlis, J., and Holmes, P., 2005. “Low-dimensional modelling of turbulence
455 using the proper orthogonal decomposition: a tutorial”. *Nonlinear Dynamics*, **41** (1), pp. 275–
456 307.
- 457 [26] Lall, S., Marsden, J. E., and Glavaški, S., 1999. “Empirical model reduction of controlled
458 nonlinear systems”. *International Federation of Automatic Control*.
- 459 [27] Lall, S., Marsden, J. E., and Glavaški, S., 2002. “A subspace approach to balanced truncation
460 for model reduction of nonlinear control systems”. *International journal of robust and nonlinear*
461 *control*, **12** (6) , pp. 519–535.
- 462 [28] Condon, M., and Ivanov, R., 2004. “Empirical balanced truncation of nonlinear systems”.
463 *Journal of Nonlinear Science*, **14** (5), pp. 405–414.

- 464 [29] Marques, F. D., and Anderson, J., 2001. “Identification and prediction of unsteady transonic
465 aerodynamic loads by multi-layer functionals”. *Journal of Fluids and Structures*, **15** (1), pp. 83–
466 106.
- 467 [30] Lucia, D. J., Beran, P. S., and Silva, W. A., 2004. “Reduced-order modeling: new approaches
468 for computational physics”. *Progress in Aerospace Sciences*, **40** (1), pp. 51–117.
- 469 [31] Brunovsky, P., 1993. “Theory of invariant manifolds and its applications to differential equa-
470 tions”. *UTMS 93*, **41**, pp. 93–41.
- 471 [32] Nouy, A., 2010. “A priori model reduction through proper generalized decomposition for solving
472 time-dependent partial differential equations”. *Computer Methods in Applied Mechanics and
473 Engineering*, **199** (23) , pp. 1603–1626.
- 474 [33] Chevreuril, M., and Nouy, A., 2012. “Model order reduction based on proper generalized de-
475 composition for the propagation of uncertainties in structural dynamics”. *International Journal
476 for Numerical Methods in Engineering*, **89** (2), pp. 241–268.
- 477 [34] Chinesta, F., Ammar, A., and Cueto, E., 2010. “Recent advances and new challenges in the
478 use of the proper generalized decomposition for solving multidimensional models”. *Archives of
479 Computational methods in Engineering*, **17** (4), pp. 327–350.
- 480 [35] Pruliere, E., Chinesta, F., and Ammar, A., 2010. “On the deterministic solution of multid-
481 dimensional parametric models using the proper generalized decomposition”. *Mathematics and
482 Computers in Simulation*, **81** (4), pp. 791–810.
- 483 [36] Ladevèze, P., and Chamoin, L., 2011. “On the verification of model reduction methods based
484 on the proper generalized decomposition”. *Computer Methods in Applied Mechanics and En-
485 gineering*, **200** (23) , pp. 2032–2047.
- 486 [37] Chinesta, F., Ladeveze, P., and Cueto, E., 2011. “A short review on model order reduction based
487 on proper generalized decomposition”. *Archives of Computational Methods in Engineering*, **18**
488 (4), p. 395.
- 489 [38] Shaw, S., and Pierre, C., 1991. “Non-linear normal modes and invariant manifolds”. *Journal
490 of sound and Vibration*, **150** (1), pp. 170–173.
- 491 [39] Pesheck, E., Pierre, C., and Shaw, S. W., 2002. “Modal reduction of a nonlinear rotating beam
492 through nonlinear normal modes*”. *Journal of vibration and Acoustics*, **124** (2), pp. 229–236.
- 493 [40] Kerschen, G., Peeters, M., Golinval, J.-C., and Vakakis, A. F., 2009. “Nonlinear normal modes,
494 part i: A useful framework for the structural dynamicist”. *Mechanical Systems and Signal
495 Processing*, **23** (1), pp. 170–194.
- 496 [41] Grolet, A., and Thouverez, F., 2015. “Computing multiple periodic solutions of nonlinear vi-
497 bration problems using the harmonic balance method and groebner bases”. *Mechanical Systems
498 and Signal Processing*, **52**, pp. 529–547.
- 499 [42] Mohammadali, M., and Ahmadian, H., 2014. “Efficient model order reduction of structural
500 dynamic systems with local nonlinearities under periodic motion”. *Shock and Vibration*, **2014**.

- 501 [43] Blanc, F., Touzé, C., Mercier, J.-F., Ege, K., and Ben-Dhia, A.-S. B., 2013. “On the numerical
502 computation of nonlinear normal modes for reduced-order modelling of conservative vibratory
503 systems”. *Mechanical Systems and Signal Processing*, **36** (2), pp. 520–539.
- 504 [44] Wang, Y., Palacios, R., and Wynn, A., 2015. “A method for normal-mode-based model reduc-
505 tion in nonlinear dynamics of slender structures”. *Computers & Structures*, **159**, pp. 26–40.
- 506 [45] Amabili, M., Sarkar, A., and Paidoussis, M., 2003. “Reduced-order models for nonlinear vibra-
507 tions of cylindrical shells via the proper orthogonal decomposition method”. *Journal of Fluids
508 and Structures*, **18** (2), pp. 227–250.
- 509 [46] Kerschen, G., Feeny, B., and Golinval, J.-C., 2003. “On the exploitation of chaos to build
510 reduced-order models”. *Computer Methods in Applied Mechanics and Engineering*, **192** (13) ,
511 pp. 1785–1795.
- 512 [47] Vakakis, A. F., Gendelman, O. V., Bergman, L. A., McFarland, D. M., Kerschen, G., and Lee,
513 Y. S., 2008. *Nonlinear targeted energy transfer in mechanical and structural systems*, vol. 156.
514 Springer Science & Business Media.
- 515 [48] Kuether, R. J., Deaner, B. J., Hollkamp, J. J., and Allen, M. S., 2015. “Evaluation of geo-
516 metrically nonlinear reduced-order models with nonlinear normal modes”. *AIAA Journal*,
517 pp. 1–13.
- 518 [49] Wang, X., 2010. “Construction of frequency-energy plots for nonlinear dynamical systems from
519 time-series data”.
- 520 [50] Peter, S., Grundler, A., Reuss, P., Gaul, L., and Leine, R. I., 2016. “Towards finite ele-
521 ment model updating based on nonlinear normal modes”. In *Nonlinear Dynamics, Volume 1*.
522 Springer, pp. 209–217.
- 523 [51] Vakakis, A. F., Manevitch, L. I., Mikhlin, Y. V., Pilipchuk, V. N., and Zevin, A. A., 1996.
524 *Normal modes and localization in nonlinear systems*. Springer.
- 525 [52] Ilbeigi, S., and Chelidze, D., 2016. “Reduced order models for systems with disparate spatial
526 and temporal scales”. In *Rotating Machinery, Hybrid Test Methods, Vibro-Acoustics & Laser
527 Vibrometry, Volume 8*. Springer, pp. 447–455.
- 528 [53] Chelidze, D., 2014. “Identifying robust subspaces for dynamically consistent reduced-order
529 models”. In *Nonlinear Dynamics, Volume 2*. Springer, pp. 123–130.
- 530 [54] Chelidze, D., and Zhou, W., 2006. “Smooth orthogonal decomposition-based vibration mode
531 identification”. *Journal of Sound and Vibration*, **292** (3), pp. 461–473.
- 532 [55] Sauer, T., Yorke, J. A., and Casdagli, M., 1991. “Embedology”. *Journal of statistical Physics*,
533 **65** (3-4), pp. 579–616.
- 534 [56] Kennel, M. B., Brown, R., and Abarbanel, H. D., 1992. “Determining embedding dimension
535 for phase-space reconstruction using a geometrical construction”. *Physical review A*, **45** (6),
536 p. 3403.

Appendix A: Governing equation of mass-spring-grid system

$$\left\{ \begin{array}{l}
 m_i \ddot{x}_i + (c_i + c_{i+1}) \dot{x}_i - c_{i+1} \dot{x}_{i+1} + (k_i + k_{i+1}) x_i - \\
 k_{i+1} x_{i+1} + (k_i - k_{i+1}) a - k_i \frac{l}{l_i} (a + \Delta x_i) + \\
 k_{i+1} \frac{l}{l_{i+1}} (a + \Delta x_{i+1}) = 0 \quad \text{for } i = 1 \\
 \\
 m_i \ddot{x}_i - c_i \dot{x}_{i-1} + (c_i + c_{i+1}) \dot{x}_i - c_{i+1} \dot{x}_{i+1} - k_i x_{i-1} + \\
 (k_i + k_{i+1}) x_i - k_{i+1} x_{i+1} + (k_i - k_{i+1}) a - \\
 k_i \frac{l}{l_i} (a + \Delta x_i) + k_{i+1} \frac{l}{l_{i+1}} (a + \Delta x_{i+1}) = 0 \quad \text{for } 2 \leq i \leq n-1 \\
 \\
 m_i \ddot{x}_i - c_i \dot{x}_{i-1} + (c_i + c_{i+1}) \dot{x}_i - k_i x_{i-1} + \\
 (k_i + k_{i+1}) x_i + (k_i - k_{i+1}) a - k_i \frac{l}{l_i} (a + \Delta x_i) + \\
 k_{i+1} \frac{l}{l_{i+1}} (a + \Delta x_{i+1}) = 0 \quad \text{for } i = n
 \end{array} \right. \quad (15)$$

$$\left\{ \begin{array}{l}
 m_i \ddot{y}_i + (c_i + c_{i+1}) \dot{y}_i - c_{i+1} \dot{y}_{i+1} + (k_i + k_{i+1}) y_i - \\
 k_{i+1} y_{i+1} - k_i \frac{l}{l_i} \Delta y_i + k_{i+1} \frac{l}{l_{i+1}} \Delta y_{i+1} = F_{y,i}(t) \quad \text{for } i = 1 \\
 \\
 m_i \ddot{y}_i - c_i \dot{y}_{i-1} + (c_i + c_{i+1}) \dot{y}_i - c_{i+1} \dot{y}_{i+1} - k_i y_{i-1} + \\
 (k_i + k_{i+1}) y_i - k_{i+1} y_{i+1} - k_i \frac{l}{l_i} \Delta y_i + \\
 k_{i+1} \frac{l}{l_{i+1}} \Delta y_{i+1} = F_{y,i}(t) \quad \text{for } 2 \leq i \leq n-1 \\
 \\
 m_i \ddot{y}_i - c_i \dot{y}_{i-1} + (c_i + c_{i+1}) \dot{y}_i - k_i y_{i-1} + \\
 (k_i + k_{i+1}) y_i - k_i \frac{l}{l_i} \Delta y_i + k_{i+1} \frac{l}{l_{i+1}} \Delta y_{i+1} = F_{y,i}(t) \quad \text{for } i = n
 \end{array} \right. \quad (16)$$

538 where a is the initial distance between the masses, l is the free length of the springs, $l_i = \sqrt{(a + \Delta x_i)^2 + (\Delta y_i)^2}$,
539 and Δx_i and Δy_i and are given as follows:

$$\Delta x_i = \begin{cases} x_i & \text{for } i = 1 \\
 x_i - x_{i-1} & \text{for } 2 \leq i \leq n \\
 -x_{i-1} & \text{for } i = n+1 \end{cases} \quad (17)$$

540

$$\Delta y_i = \begin{cases} y_i & \text{for } i = 1 \\
 y_i - y_{i-1} & \text{for } 2 \leq i \leq n \\
 -y_{i-1} & \text{for } i = n+1 \end{cases} \quad (18)$$

541 We should note that here only linear damping is considered for the system.